Investigation of Energy-Band Structures and Electronic Properties of PbS and PbSe*

SOHRAB RABII†
Materials Theory Group, Department of Electrical Engineering, Massachusetts Institute of Technology, Cambridge, Massachusetts

(Received 21 July 1967: revised manuscript received 8 November 1967)

The augmented-plane-wave method is used to calculate the energy-band structure of PbS and PbSe. The relativistic mass-velocity, Darwin, and spin-orbit interaction corrections are taken into account. The resulting wave functions are used to calculate the matrix elements of momentum, which are then used in a $\mathbf{k}\cdot\mathbf{p}$ perturbation scheme to obtain effective masses and g factors. Previous calculation of g factors for PbTe is corrected. The effect of strain on energy bands of PbS and PbSe is calculated using the deformation-potential theory. The energy bands obtained, as well as the calculated electronic properties of these materials, are in good agreement with other theoretical and experimental investigations.

I. INTRODUCTION

THE electronic properties of the lead salts have been the subject of numerous and extensive experimental studies. Interpretation of these results is greatly facilitated by the availability of a reliable energy-band calculation. Such a first-principles calculation for PbTe was carried out by Conklin *et al.*[1] using the augmented-plane-wave (APW) method, and the results were in very good agreement with experiment. Subsequently, Pratt *et al.*[2] and Ferreira[3] utilized these results to calculate some electronic properties of PbTe.

Another theoretical study of the band structure of these materials using the pseudopotential method has been carried out by Lin and Kleinman.[4] However, this method involves five arbitrary constants whose values must be determined by fitting the bands to certain experimental data, while in the APW method there is at most, only one parameter, the energy gap, which has to be determined by experiment. Furthermore, the necessity of this adjustment is not an inherent feature of the APW method and is due to a peculiarity of the lead salts, namely, their small forbidden gap and the nature of the conduction-band charge distribution. Lin and Kleinman and Pratt and Ferreira utilized their wave functions in a $\mathbf{k}\cdot\mathbf{p}$ analysis to calculate effective masses and g factors for the lead salts. However, in both cases they neglected to take into account some significant terms in the transverse g factor .

Dimmock and Wright[5] have made an analysis of the band-edge structure of the lead salts based on the nearly-free-electron model and havea rrived at a model involving three levels for the conduction band and three for the valence band. They reduced the possible arrangements of these levels to fourteen distinct cases. Furthermore, they carried out a parameterized $\mathbf{k}\cdot\mathbf{p}$ perturbation, although they neglected the very important spin-orbit mixing of the double-group levels of the same symmetry. They predicted a value of 2 for g_1, which does not agree with experiment or the present work.

Mitchell and Wallis[6] obtained the general expressions for the effective masses and g factors for the lead salts in terms of five momentum matrix elements and two spin-orbit mixing parameters. Their spin assignment for the double-group basis functions differs from those of Dimmock and Wright,[5] Pratt and Ferreira,[2] and the present work because the three latter studies have specifically chosen a right-handed coordinate system. This difference in spin assignment leads to the reversal of the sign of g factor between Mitchell and Wallis and the rest.

The purpose of the present work is to extend the APW calculations of PbTe to PbS and PbSe and to correct the transverse g factors obtained by Pratt and Ferreira[2] for PbTe and by Lin and Kleinman[4] for all the lead salts.

As a first step, the energy bands are calculated taking into account such relativistic corrections as spin-orbit interaction, mass-velocity, and Darwin terms. The wave functions are then utilized to calculate the matrix elements of a generalized momentum operator between different states, to be used in a $\mathbf{k}\cdot\mathbf{p}$ scheme to obtain effective masses and g factors. Furthermore, the effect of strain on the energy bands is determined by calculation of the deformation potentials.

II. APW HAMILTONIAN

The Hamiltonian used in the calculations is obtained by reducing Dirac's four-component field equation to the two-component Schrödinger's equation, and has

* Based on a doctoral dissertation for degree of Doctor of Philosophy in Electrical Engineering at MIT. This research was supported in part by the U. S. Office of Naval Research.

† Present address: Central Research Department, Monsanto Company, St. Louis, Mo.

[1] J. B. Conklin, Jr., L. E. Johnson, and G. W. Pratt, Jr., Phys. Rev. **137**, A1282 (1965).

[2] G. W. Pratt, Jr., and L. G. Ferreira, in *Proceedings of the International Conference on Physics of Semiconductors* (Dunod Cie., Paris, 1964).

[3] L. G. Ferreira, Phys. Rev. **137**, A1601 (1965).

[4] P. J. Lin and L. Kleinman, Phys. Rev. **142**, 478 (1966).

[5] J. O. Dimmock and G. B. Wright, Phys. Rev. **135**, A821 (1964).

[6] D. L. Mitchell and R. F. Wallis, Phys. Rev. **151**, 581 (1966).

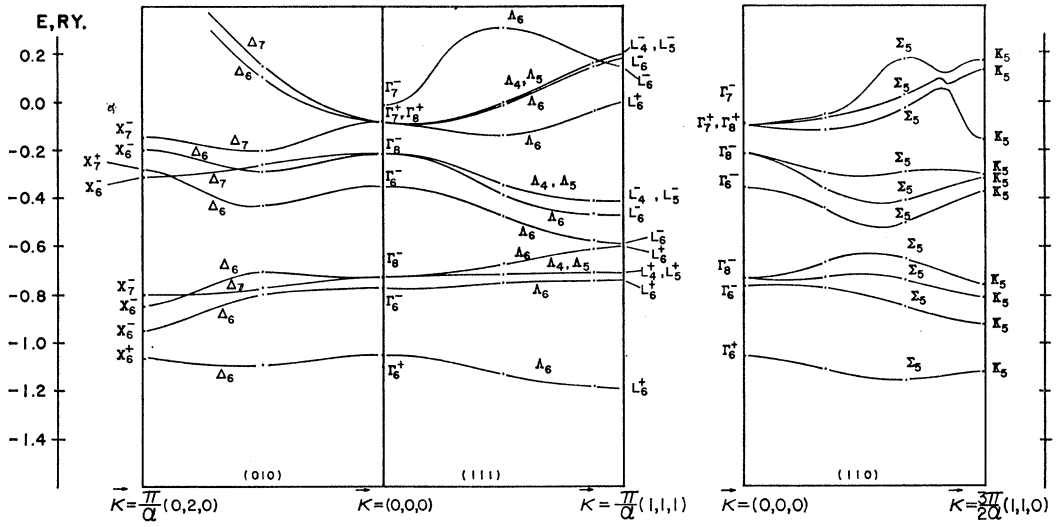

FIG. 1. Energy bands for PbS in the [111], [010], and [110] directions.

the following form:

$$\mathcal{H}=\frac{p^2}{2m}+V(\mathbf{r})+\frac{\hbar}{4m^2c^2}\boldsymbol{\sigma}[(\nabla V)\times\mathbf{p}]+\frac{\hbar^2}{8m^2c^2}(\nabla^2 V)-\frac{p^4}{8m^3c^2}. \quad (1)$$

The first two terms are the conventional kinetic- and potential-energy terms. The third term is due to the spin-orbit interaction which leads to the splitting of the single-group levels. The next two terms, the Darwin and mass-velocity corrections, do not lead to splitting of the levels, but, by imparting unequal shifts to them, lead to rearranging of their order.

The calculations were carried out in three steps. First, a Hamiltonian containing only the potential- and kinetic-energy terms was used to find the unperturbed levels. Then the Darwin and mass-velocity terms were used as perturbation on the obtained energy levels. The last step involved the inclusion of the spin-orbit term, which necessitates the introduction of spinor wave functions which form the basis for the irreducible representations of the double group.

III. ENERGY BANDS

The energy bands are calculated for the [111], [110], and [010] directions (Figs. 1 and 2). Both PbS and PbSe are direct-gap semiconductors, and the energy gap occurs in the [111] direction at point L on the face of the Brillouin zone. Note that since the two levels

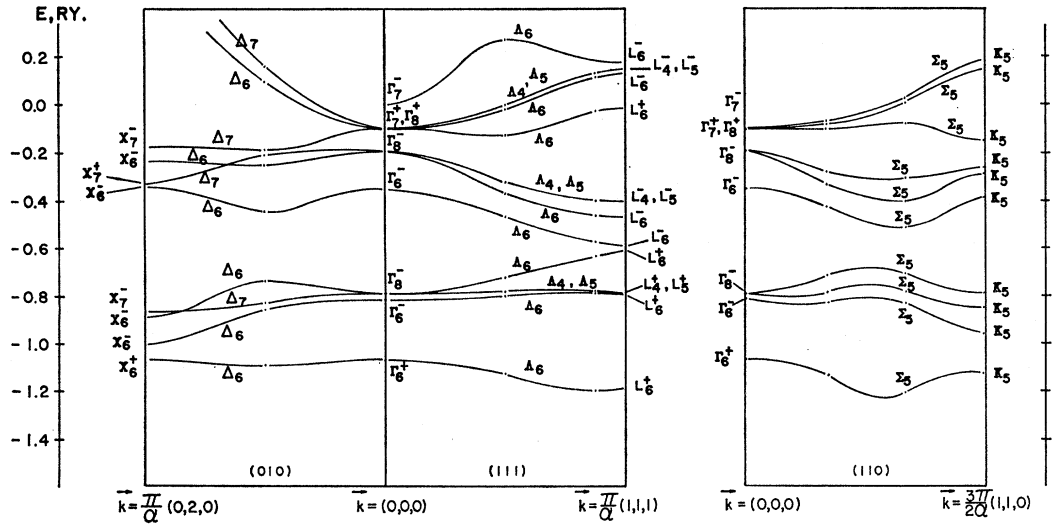

FIG. 2. Energy bands for PbSe in the [111], [010], and [110] directions.

TABLE I. Charge-density distributions for the valence- and conduction-band edges for PbS, PbSe, and PbTe at L.

PbS				
Conduction band	L_2^-	0.502 (plane-wave region)	0.342 (p type around Pb)	0.085 (s type around S)
Valence band	L_1^+	0.051 (plane-wave region)	0.369 (s type around Pb)	0.569 (p type around S)
PbSe				
Conduction band	L_2^-	0.505 (plane-wave region)	0.337 (p type around Pb)	0.091 (s type around Se)
Valence band	L_1^+	0.079 (plane-wave region)	0.379 (s type around Pb)	0.520 (p type around Se)
PbTe				
Conduction band	L_2^-	0.484 (plane-wave region)	0.309 (p type around Pb)	0.124 (s type around Te)
Valence band	L_1^+	0.177 (plane-wave region)	0.365 (s type around Pb)	0.411 (p type around Te)

L_6^- and L_6^+ which mark the forbidden energy gap are very close together, the calculated gap is the difference of two very large numbers and very sensitive to slight changes in the position of these levels. Since the L_2^- band, which under spin-orbit interaction goes into L_6^- (bottom of the conduction band), has 50% of its charge concentrated in the plane-wave region (Table I), its position is very sensitive to the value of the constant potential in this region. Thus a slight change in this value results in a "large" relative change in the size of the gap and even in the ordering of the L_6^- and L_6^+ levels. Indeed, this is the case for the initial calculations for PbSe and PbTe (Fig. 3).

However, the rest of the levels are insensitive to small changes in the constant potential. As a result, the size of the gap and the correct ordering of the L_6^- and L_6^+ levels (as indicated by experiment) can be used to choose the constant potential outside the spheres and thus impart a certain measure of self-consistency to the calculations. Figure 3 shows the shift of the conduction- and valence-band edges[1] at L for PbS, PbSe, and PbTe due to the different relativistic corrections, before adjusting the size of the gap or the order of L_6^- and L_6^+. The changes are seen to be very significant, and neglecting them would result in a totally inaccurate band picture.

A comparison of the band edge[1] at L for PbS, PbSe, and PbTe (Fig. 4) shows a general trend in the movement of bands which follows that of the atomic numbers S, Se, and Te. The uppermost complex (L_6^-, L_4^-, L_5^-) comes from the splitting of the doubly degenerate single-group state L_3^-. The spin-orbit splitting of L_3^- in the conduction band is much larger than that of L_3^+ in the valence band because L_3^- is p type centered around Pb atoms (Table I), and therefore the splitting is mainly due to the spin-orbit effect in Pb, which is large. However, L_3^+ is primarily p type about S, Se, or Te, and thus its splitting is smaller than that of L_3^-. For exactly the same reason, the splitting of the L_3^+ level decreases as we move from Te to Se and finally to S, because of the decrease in the size of atoms.

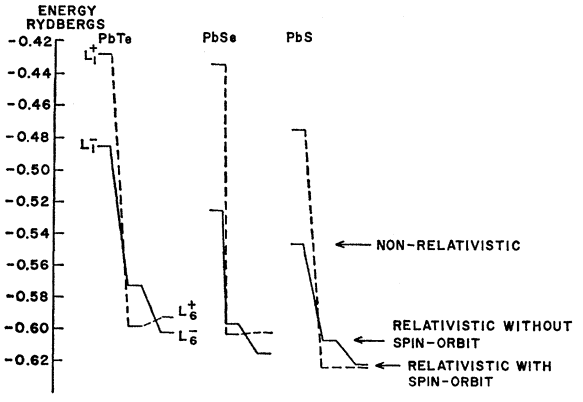

FIG. 3. Relativistic effects on the band edges of PbS, PbSe, and PbTe. (The order of L_6^- and L_6^+ for PbSe and PbTe are reversed in the final results.)

IV. k·p PERTURBATION

Using the effective-mass approximation of Luttinger and Kohn[7] and the formalism of Roth,[8] the following matrix element of the effective Hamiltonian in the presence of magnetic field can be obtained:

$$\langle\Phi_{n\kappa i}|\mathcal{H}_{\text{eff}}|\Phi_{n\kappa j}\rangle=\left(E_n^0+\frac{\hbar^2K^2}{2m}\right)\delta_{ij}+\kappa\sum_\mu\frac{\pi_{i\mu}\cdot\pi_{\mu j}}{E_n^0-E_\mu^0}\kappa$$
$$+2\mu_\beta\mathbf{S}_{ij}\cdot\mathbf{H}-\frac{ieh}{2m^2c}\mathbf{H}\sum\frac{\pi_{i\mu}\times\pi_{\mu j}}{E_n^0-E_\mu^0}, \quad (2)$$

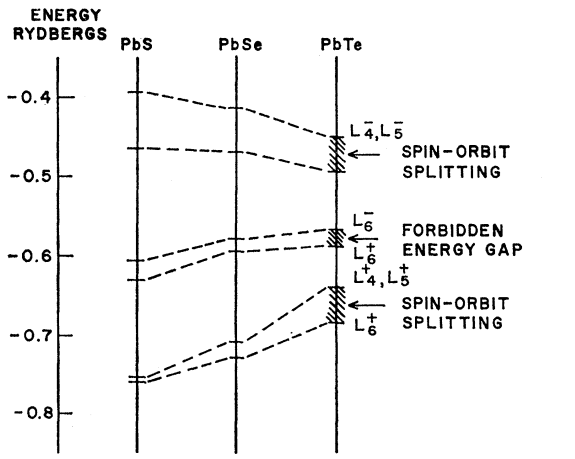

FIG. 4. Comparison of the energy levels at point L for PbS, PbSe, and PbTe.

[7] J. M. Luttinger and W. Kohn, Phys. Rev. **97**, 869 (1955).
[8] L. M. Roth, Phys. Rev. **118**, 1534 (1960).

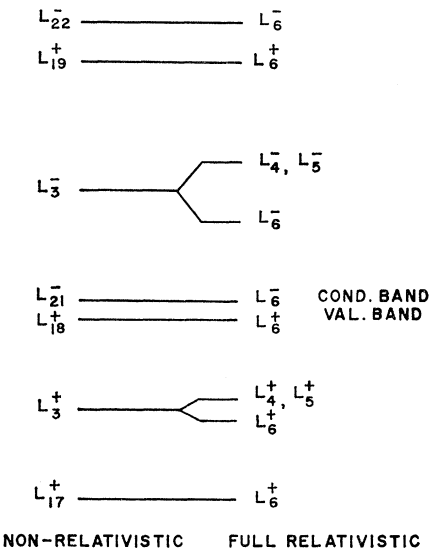

FIG. 5. Energy levels taken into account for the $\mathbf{k}\cdot\mathbf{p}$ perturbation.

where

$$\pi=\mathbf{p}+\frac{\hbar}{4mc^2}\sigma\times(\nabla V)-\frac{1}{2m^2c^2}(p^2)\mathbf{p}-\frac{1}{2m^2c^2}(\mathbf{P}\cdot\mathbf{p})\mathbf{p}-\frac{1}{4m^2c^2}(p^2)\mathbf{P}. \quad (3)$$

The operator $\mathbf{P}=\mathbf{p}+(e\mathbf{A}/c)$ operates on the exponent part of $\Phi_{n\kappa i}$ and $\mathbf{p}$ operates on the Bloch-function part only. In the above relations, terms of the order $\mathbf{P}^3$ and A^2 or higher are neglected. $\mathbf{S}_{ij}$ and π_{ij} are the matrix elements of electron spin and π between the band-edge wave functions, μ_β is the Bohr magneton, and $\{\ \}$ denotes the anticommutator. The expression for π contains the relativistic corrections explicitly.

Figure 5 shows the energy levels that enter into the $\mathbf{k}\cdot\mathbf{p}$ calculation. The two upper levels L_6^-, L_6^+ and the lowest-level L_6^+ are not included in the sum over μ in Eq. (2), since their energy separations from the valence- and conduction-band complex are of the order of 0.6 Ry or higher. However, because of the spin-orbit mixing, the two levels comprising valence and conduction bands are a mixture of all levels which have L_6^+ and L_6^- symmetries, respectively. Since there are more than one L_1^+ and L_2^- single-group levels, a second subscript is used to differentiate between these levels. The sub-

TABLE II. Composition of levels used in the $\mathbf{k}\cdot\mathbf{p}$ perturbation.

$|L_4^-,1\rangle=D|L_4^-(L_3^-)\rangle$
$|L_{61}^-,2\rangle=C_1|L_{61}^-(L_3^-)\rangle+C_2|L_{61}^-(L_{21}^-)\rangle$
$|L_{61}^-,c\rangle=A_1|L_{61}^-(L_{21}^-)\rangle+A_2|L_{61}^-(L_{22}^-)\rangle+A_3|L_{61}^-(L_3^-)\rangle$
$|L_{61}^+,v\rangle=B_1|L_{61}^+(L_{17}^+)\rangle+B_2|L_{61}^+(L_{18}^+)\rangle+B_3|L_{61}^+(L_{19}^+)\rangle+B_4|L_{61}^+(L_3^+)\rangle$
$|L_{61}^+,4\rangle=E_1|L_{61}^+(L_3^+)\rangle+E_2|L_{61}^+(L_{18}^+)\rangle$
$|L_4^+,3\rangle=F|L_4^+(L_3^+)\rangle$

TABLE III. Coefficients of spin-orbit mixing for the levels used in the $\mathbf{k}\cdot\mathbf{p}$ perturbation. The mixing coefficients of Lin and Kleinman are given by a, b, c, and d, and correspond to B_2, B_4, A_1, and A_3, respectively.

	PbS	PbSe	PbTe
A_1	$0.456+0.823i$	0.920	−0.807
A_2	$0.040+0.072i$	−0.100	
A_3	$-0.157-0.284i$	0.374	0.568
B_1	−0.225	−0.228	
B_2	−0.968	−0.966	0.948
B_3	−0.110	0.077	
B_4	0.018	0.098	0.228
C_1	$-0.924-0.175i$	0.921	0.815
C_2	$-0.325-0.061i$	−0.381	0.574
D	$0.484+0.874i$	1.000	1.000
E_1	1.000	−1.000	−0.973
E_2			0.226
F	1.000	−1.000	1.000
a	0.999	0.999	0.974
b	0.032	0.041	0.227
c	0.881	0.864	0.668
d	0.473	0.504	0.744

TABLE IV. Single-group matrix elements of momentum for the lead salts.

	PbS	PbS extrapolation	PbSe	PbTe[a]
$M_{17,21^z}$	−0.583	−0.559	0.575	
$M_{18,21^z}$	0.501	0.483	−0.458	−0.319
$M_{19,21^z}$	−0.280	−0.282	−0.463	
$M_{17,22^z}$	0.396	0.337	0.318	
$M_{18,22^z}$	1.057	0.918	0.924	
$M_{19,22^z}$	−0.985	−1.028	0.625	
$M_{3,21^y}$	−0.872	−0.813	0.939	−1.012
$M_{3,22^y}$	−0.022	−0.022	−0.019	
M_{33^z}	−0.408	−0.385	−0.420	−0.416
M_{33^y}	0.771	0.719	0.792	0.798
$M_{17,3^y}$	−0.075	−0.081	−0.122	
$M_{18,3^y}$	0.896	0.858	1.024	−1.121
$M_{19,3^y}$	1.010	0.940	−1.315	

[a] Reference 2.

TABLE V. Double-group momentum matrix elements of spin-orbit-mixed bands.

$\langle L_{61}^+v|\pi_z|L_{61}^-c\rangle=A_1(B_1^*M_{17,21^z}+B_2^*M_{18,21^z}+B_3^*M_{19,21^z})+A_2(B_1^*M_{17,22^z}+B_2^*M_{18,22^z}+B_3^*M_{19,22^z})+A_3B_4^*M_{33^z}$

$\langle L_{61}^+v|\pi_x|L_{62}^-c\rangle=-\frac{1}{2}\sqrt{2}A_3^*(B_1^*M_{17,3^y}+B_2^*M_{18,3^y}+B_3^*M_{19,3^y})+\frac{1}{2}\sqrt{2}B_4^*(A_1^*M_{21,3^y}+A_2^*M_{22,3^y})$

$\langle L_{61}^+v|\pi_z|L_{61}^-,2\rangle=C_2(B_1^*M_{17,21^z}+B_2^*M_{18,21^z}+B_3^*M_{19,21^z})+B_4^*C_1M_{33^z}$

$\langle L_{61}^+v|\pi_z|L_{62}^-,2\rangle=-\frac{1}{2}\sqrt{2}C_1^*(B_1^*M_{17,3^y}+B_2^*M_{18,3^y}+B_3^*M_{19,3^y})+\frac{1}{2}\sqrt{2}C_2^*B_4^*M_{21,3^y}$

$\langle L_{61}^+v|\pi_x|L_4^-,1\rangle=-\frac{1}{2}iD(B_1^*M_{17,3^y}+B_2^*M_{18,3^y}+B_3^*M_{19,3^y})-\frac{1}{2}\sqrt{2}DB_4^*M_{33^y}$

$\langle L_{61}^-c|\pi_z|L_{61}^+,4\rangle=A_3^*E_1M_{33^z}+E_2(A_1^*M_{18,21^z}+A_2^*M_{18,22^z})$

$\langle L_{61}^+v|\pi_x|L_5^-,1\rangle=-\frac{1}{2}D^*(B_1^*M_{17,3^y}+B_2^*M_{18,3^y}+B_3^*M_{19,3^y})-\frac{1}{2}\sqrt{2}iD^*B_4^*M_{33^y}$

$\langle L_{61}^-c|\pi_x|L_{62}^+,4\rangle=\frac{1}{2}\sqrt{2}Ei^*(A_1^*M_{21,3^y}+A_2^*M_{22,3^y})-\frac{1}{2}\sqrt{2}E_2^*A_3^*M_{18,3^y}$

$\langle L_{61}^-c|\pi_x|L_4^+,3\rangle=-\frac{1}{2}iF(A_1^*M_{21,3^y}+A_2^*M_{22,3^y})+\frac{1}{2}\sqrt{2}FA_3^*M_{33^y}$

$\langle L_{61}^-c|\pi_x|L_5^+,3\rangle=-\frac{1}{2}F^*(A_1^*M_{21,3^y}+A_2^*M_{22,3^y})-\frac{1}{2}\sqrt{2}iFA_3^*M_{33^y}$

TABLE VI. Calculated values of the double-group momentum matrix elements for spin-orbit-mixed bands ($\pi' = \pi/m_0$).

	PbS	PbSe	PbTe	PbS extrapolation
$\langle L_{61}^+v \vert \pi_x' \vert L_{61}^-c\rangle$	$-0.186-0.336i$	0.331	0.190	$-0.176-0.318i$
$\langle L_{61}^+v \vert \pi_x' \vert L_{62}^-c\rangle$	$-0.112-0.202i$	0.341	0.559	$-0.107+0.193i$
$\langle L_{61}^+v \vert \pi_z' \vert L_{61}^-,2\rangle$	$0.112+0.021i$	-0.143	-0.251	$0.108+0.020i$
$\langle L_{61}^+v \vert \pi_x' \vert L_{62}^-,2\rangle$	$-0.624+0.118i$	0.669	-0.519	$-0.595+0.112i$
$\langle L_{61}^+v \vert \pi_x' \vert L_4^-,1\rangle$	$-0.435+0.224i$	$-0.055+0.531i$	$-0.129+0.531i$	$-0.404+0.213i$
$\langle L_{61}^+v \vert \pi_x' \vert L_5^-,1\rangle$	$0.224-0.435i$	$-0.531-0.055i$	$0.531-0.129i$	$0.213-0.404i$
$\langle L_{61}^-c \vert \pi_z' \vert L_{61}^+,4\rangle$	$0.064-0.116i$	0.157	0.288	$0.060-0.107i$
$\langle L_{61}^-c \vert \pi_x' \vert L_{62}^+,4\rangle$	$-0.281+0.509i$	0.612	-0.460	$-0.263+0.475i$
$\langle L_{61}^-c \vert \pi_x' \vert L_4^+,3\rangle$	$0.274+0.354i$	$-0.209+0.433i$	$0.320-0.408i$	$0.256+0.330i$
$\langle L_{61}^-c \vert \pi_x' \vert L_5^+,3\rangle$	$0.044-0.446i$	$0.433-0.209i$	$-0.408+0.320i$	$0.042-0.416i$

script coincides with the number of the spinor function in the spin-orbit secular equation which arises from the particular single-group level.

In order to obtain a diagonal effective-mass tensor, a coordinate system is chosen with x, y, z axes along the $[\bar{1}\bar{1}2]$, $[1\bar{1}0]$, and $[111]$ directions, respectively. The double-group basis functions used are those given by Pratt and Ferreira.[2] Note that they obtained these basis functions from Conklin,[9] who employed the above coordinate system. Pratt and Ferreira,[2] through an oversight, have given a different set of coordinates, a fact that did not have any effect on their results.

Tables II and III show the spin-orbit mixing of the levels included in the sum over μ in Eq. (2). For the purpose of comparison, the equivalent mixing parameters of Lin and Kleinman[4] and their numerical values are given. In the present work, a mixing of three levels for conduction band and four levels for the valence band have been used, as compared to two-level mixing for both bands by Lin and Kleinman[4] and Conklin *et al.*[1] This is the reason for the slight difference of the two major mixing parameters of the present work and that of Lin and Kleinman for PbS and PbSe. In the case of PbTe, the model used by Lin and Kleinman places the $L_6^-(L_3^-)$ below $L_6^-(L_2^-)$ in the conduction-band complex, which explains the difference between their results and those of Conklin *et al.*[1] and Pratt and Ferreira.[2]

The symmetry properties of the single-group basis functions dictate the following relationships among the matrix elements of π:

$$\begin{aligned}
&\langle L_{31}^- \vert \pi_y \vert L_{32}^+\rangle = \langle L_{32}^- \vert \pi_y \vert L_{31}^+\rangle = \langle L_{31}^- \vert \pi_x \vert L_{31}^+\rangle \\
&\qquad = -\langle L_{32}^- \vert \pi_x \vert L_{32}^+\rangle = -im_0 M_{33}^y, \\
&\langle L_{31}^- \vert \pi_z \vert L_{31}^+\rangle = \langle L_{32}^- \vert \pi_z \vert L_{32}^+\rangle = -im_0 M_{33}^z, \\
&\langle L_1^+ \vert \pi_z \vert L_2^-\rangle = im_0 M_{12}^z, \qquad (4) \\
&\langle L_2^- \vert \pi_x \vert L_{32}^+\rangle = \langle L_2^- \vert \pi_y \vert L_{31}^+\rangle = -im_0 M_{23}^y, \\
&\langle L_1^+ \vert \pi_x \vert L_{32}^-\rangle = \langle L_1^+ \vert \pi_y \vert L_{31}^-\rangle = im_0 M_{13}^y.
\end{aligned}$$

The remainder of the matrix elements of π between these states are identically zero. The matrix elements are calculated (Table IV) using the computer programs developed by Ferreira for the case of PbTe. Since only ten APW's were used in the expansion of the wave functions in the above calculations, the convergence of some of the matrix elements was not too satisfactory. An extrapolation was performed on the values of the matrix elements for PbS; however, as it turns out later, these new values do not make a substantial difference in the effective masses and g factors.

Table V lists the independent nonzero matrix elements of the π operator between the final spin-orbit-mixed levels. The matrix elements not listed are either zero or can be obtained from the given elements by the application of relationships obtainable from the time-reversal symmetry and the point-group symmetry of the group of k vector. Table VI gives the numerical values of the above matrix elements for PbS, PbSe, and extrapolated PbS. The Slater system of atomic units was used in the calculation, where the unit of length is the radius of the first Bohr orbit of hydrogen, unit of mass is twice that of free electron, and unit of angular momentum is $\hbar$. In order to facilitate the numerical calculations, the matrix elements of π/m_0 were calculated instead of π.

Tables XII and XIII give the calculated effective masses and g factors for the conduction and valence bands of these materials. Since, because of spin-orbit mixing, the conduction and valence bands are not purely of one spin, and since there are no direct experimental determinations of sign of the g factors, no effect has been made to define a sign for the theoretical

TABLE VII. Matrix elements of isotropic and [111] uniaxial strains in eV.

Single-group states	Isotropic		[111] direction	
	PbS	PbSe	PbS	PbSe
L_{21}^-, L_{21}^-	-5.51	-5.75	1.23	1.29
L_{22}^-, L_{22}^-	⋯	-23.20	⋯	-12.65
L_{21}^-, L_{22}^-			⋯	8.00
L_3^-, L_3^-	-8.73	-9.08	3.10	2.77
L_{17}^+, L_{17}^+	7.24	6.91	-0.61	-0.79
L_{18}^+, L_{18}^+	-24.83	-24.45	-8.38	-5.73
L_{19}^+, L_{19}^+	-15.82	-14.84	-8.92	-4.06
L_{17}^+, L_{18}^+			1.39	1.53
L_{17}^+, L_{19}^+			0.44	2.09
L_{19}^+, L_{18}^+			8.73	-2.75
L_3^+, L_3^+	-5.07	-5.78	0.25	0.48

[9] J. B. Conklin, Jr., Ph.D. thesis, MIT, 1964 (unpublished).

TABLE VIII. Matrix elements of [111] and [001] uniaxial strains in eV.

Single-group states	[11$\bar{1}$] direction PbS	PbSe	Single-group states	[001] direction PbS	PbSe
$L_1^{R-}(L_3^-),L_1^{R-}(L_3^-)$	−1.52	−1.77	$L_1^{T-}(L_3^-),L_1^{T-}(L_3^-)$	−1.13	0.91
$L_2^{R-}(L_{21}^-),L_2^{R-}(L_3^-)$	−3.46	3.15	$L_2^{T-}(L_{21}^-),L_2^{T-}(L_3^-)$	−5.12	4.58
$L_2^{R-}(L_{22}^-),L_2^{R-}(L_3^-)$	···	3.68	$L_2^{T-}(L_{22}^-),L_2^{T-}(L_3^-)$	···	2.32
$L_1^{R+}(L_3^+),L_1^{R+}(L_3^+)$	−3.26	−3.87	$L_1^{T+}(L_3^+),L_1^{T+}(L_3^+)$	−3.42	−3.93
$L_1^{R+}(L_{17}^+),L_1^{R+}(L_3^+)$	−0.12	−0.24	$L_1^{T+}(L_{17}^+),L_1^{T+}(L_3^+)$	−2.85	−3.17
$L_1^{R+}(L_{18}^+),L_1^{R+}(L_3^+)$	1.08	1.88	$L_1^{T+}(L_{18}^+),L_1^{T+}(L_3^+)$	5.84	6.33
$L_1^{R+}(L_{19}^+),L_1^{R+}(L_3^+)$	6.70	−5.66	$L_1^{T+}(L_{19}^+),L_1^{T+}(L_3^+)$	4.64	−5.52

g factors. Nevertheless, it should be stated that the valence and conduction bands have g factors of opposite sign, in agreement with other published works.

V. EFFECT OF STRAIN ON ENERGY BANDS

A theoretical study of the effect of strain on crystals with NaCl structure was first made by Pikus and Bir,[10,11] and deductions regarding the energy-band structure of PbTe and PbSe were made from experimental data. Subsequently, Ferreira[3] adapted the theory of Bir and Pikus to the specific case of PbTe by treating the strain as a perturbation on the APW energy bands of PbTe. This theory is applied to the case of PbS and PbSe in the present work.

It was shown by Ferreira that for a cubic crystal, the uniaxial strains along [001], [111], and [11$\bar{1}$] axes are sufficient to describe the behavior of the bands under a general strain. For this reason and since the energy gap in the lead salts occurs at L, we shall limit the calculation to point L and the above-mentioned strains. The strain Hamiltonian has nonzero matrix elements only between the representations that contain a common irreducible representation of the subgroup created by the application of strain. Tables VII and VIII give the matrix elements of the isotropic and the three uniaxial strains [111], [11$\bar{1}$], and [001] between the single-group levels. The superscripts R and T denote the rhombohedral [11$\bar{1}$] and the tetragonal [001] strains, respectively. Table IX gives the deformation-potential constants for the single-group levels of PbS and PbSe in units of eV. Finally, the deformation potentials for the spin-orbit-mixed valence and conduction bands are given in Table X.

TABLE IX. Deformation-potential constants for the single-group levels of PbS and PbSe in units of eV.

Single-group levels	D_u PbS	PbSe	D_d PbS	PbSe	D_{ISO} PbS	PbSe
L_{21}^-	4.60	4.81	−3.37	−3.52	− 5.71	− 5.75
L_{22}^-		−7.37		−5.27		−23.20
L_3^-	9.01	8.69	−5.91	−5.92	− 8.73	− 9.08
L_{17}^+	−4.53	−4.64	3.92	3.85	7.24	6.91
L_{18}^+	−0.15	3.63	−8.22	−9.36	−24.83	−24.45
L_{19}^+	−5.46	1.33	−3.45	−5.39	−15.83	−14.84
L_3^+	3.91	3.61	−2.66	−3.13	− 5.07	− 5.78

[10] G. E. Pikus and G. L. Bir, Fiz. Tverd. Tela **4**, 2090 (1962) [English transl.: Soviet Phys.—Solid State **8**, 1530 (1963)].

[11] G. L. Bir and G. E. Pikus, Fiz. Tverd. Tela **1**, 1642 (1959) [English transl.: Soviet Phys.—Solid State **1**, 1502].

VI. COMPARISON WITH EXPERIMENT AND DISCUSSION

A. Bands

The bulk of the experimental data on lead salts indicate the existence of a direct minimum energy gap in the [111] direction at point L on the face of the Brillouin zone. Furthermore, they indicate that both the valence and conduction bands are made of four equivalent prolate ellipsoids of revolution with their axes along the ⟨111⟩ directions. These deductions fit exactly the theoretical results. Reflectivity measurements by Cardona and Greenaway[12] are consistent with the ordering and symmetries of the conduction and valence bands. Because of the large number of theoretically allowable transitions, a one-to-one matching of experimental and theoretical transitions is not possible until the strength of the possible transitions has been calculated theoretically.

TABLE X. Deformation potential for valence and conduction bands of the lead salts in eV.

	D_u (conduction)	D_d (conduction)	D_u (valence)	D_d (valence)	D_{ISO} (conduction −valence)
PbS	5.01	−3.60	3.25	−8.75	17.21
PbSe	2.56	−2.67	4.67	−9.15	17.24
PbTe[a]	8.29	−4.36	10.46	−9.83	11.55

[a] Reference 3.

TABLE XI. Comparison of certain energy gaps (in eV) with those given by Lin and Kleinman (Ref. 4). The values for E_0 are from Mitchell and Wallis (Ref. 6).

	Lin and Kleinman PbTe	PbSe	PbS	Present work PbTe	PbSe	PbS
E_0	0.014	0.012	0.021	0.014	0.012	0.012
E_1	0.091	0.113	0.136	0.078	0.110	0.138
E_2	0.180	0.229	0.269	0.191	0.260	0.319
E_3	0.257	0.331	0.390	0.389	0.419	0.499
E_4	0.463	0.522	0.596	0.611	0.704	0.710
E_5	0.573	0.669	0.721	0.739	0.846	0.874

[12] M. Cardona and D. L. Greenaway, Phys. Rev. **133**, A1685 (1964).

TABLE XII. Comparison of calculated effective masses with experiment.

		m_t^*/m_0		m_l^*/m_0		$K=m_l^*/m_t^*$		E_g (eV)[a]
	Theory	Experiment	Theory	Experiment	Theory	Theory	Experiment	
PbTe	Conduction	0.033	0.024	0.236	0.24	7.15	10	0.19
	Valence	0.030	0.022	0.419	0.31	13.98	14	
PbSe	Conduction	0.061	0.040	0.097	0.070	1.59	1.75	0.16
	Valence	0.062	0.034	0.120	0.068	1.94	2.0	
PbS	Conduction	0.138	0.080	0.123	0.105	0.89	1.3	0.28
	Valence	0.145	0.075	0.163	0.105	1.12	1.4	
PbS extrapolated	Conduction	0.154		0.136		0.88		
	Valence	0.166		0.186		1.12		

[a] Reference 15.

Nevertheless, a comparison of certain possible transitions with those of Lin and Kleinman[4] are given in Table XI. The labels correspond to the identification made by Lin and Kleinman with the experimental transitions of Cardona and Greenaway.[12] These identifications are not felt to be conclusive, especially in light of the fact that some of the experimental values were used by Lin and Kleinman to fix the disposable constants in their pseudopotential. The energy-band structures of the lead salts calculated by Lin and Kleinman agree very well in their qualitative features and in some of the quantitative details, with those obtained by the APW method.

Sacks and Spicer[13] have carried out photoemission measurements on PbS, and their results indicate the existence of a flat band at 2.0 eV below the top of the valence band, which compares excellently with the L_4^+, L_5^+, and L_6^+ complex arising from the L_3^+ single-group state and situated at 2.1 eV below the top of the valence band. Furthermore, the resolution of their experimental apparatus sets a limit of 0.1 eV on the splitting of the L_4^+, L_5^+ levels from the L_6^+ level, which again is in agreement with the calculated results. The existence of another high density of states is observed by them at 6.5 eV above the top of the valence band, which again can be identified with a minimum in a Λ_6 band in the [111] direction located at 6.47 eV above the top of the valence band.

B. Effective Masses and *g* Factors

The experimental results for the effective masses and *g* factors are those obtained by Cuff *et al.*[14] through Shubnikov-de Haas measurements. Since their experiments were carried out in the temperature range of 1.2 to 4.2°K, the size of the energy gap measured at 4.2°K by Mitchell *et al.*[15] was used in the calculation. A second set of experimental values for *g* factors was obtained by Butler and Calawa[16] by measuring the shift in the emission peaks from diode lasers at 4.2°K with the application of a magnetic field in the [100] direction. Another set of values was obtained by Mitchell *et al.*[15] through magneto-optical studies.

Tables XII and XIII show the comparison between the theoretical and experimental results.

The theoretical values for effective masses are in general larger than the experimental values, and those of the *g* factors are smaller. However, considering the sensitiveness of the calculated results to small variations in the size of the forbidden gap, the agreement with experiment is very good. The same factor is responsible for the fact that longitudinal effective mass for the conduction band of PbS is smaller than the transverse effective mass. A slight reduction in the size of the gap will reverse this situation. As shown in the thesis, the nonparabolic approximation leads to an increase in the values for effective masses and does not improve the agreement with experiment.

TABLE XIII. Comparison of calculated *g* factors with experiment.

		$\lvert g_t\rvert$ Theory	Theory	$\lvert g_l\rvert$ Experiment[a]	Theory	$\lvert g_{100}\rvert$ Experiment[b]	Experiment[c]
PbTe	Conduction	11.80	37.88	45±8	23.90	29	
	Valence	10.02	40.01	51±8	24.50	29	
PbSe	Conduction	18.28	16.00	27±7	17.55	19	22 ±4
	Valence	15.08	18.82	32±7	16.42	19	22 ±4
PbS	Conduction	5.90	6.02	12±3	5.94	11.5	10.0±1.5
	Valence	5.38	4.18	13±3	5.01	7.0	8.5±1.5
PbS extrapolated	Conduction	5.17	5.52				
	Valence	4.67	3.74				

[a] Reference 14. [b] Reference 16. [c] Reference 15.

[13] B. H. Sacks and W. E. Spicer, Bull. Am. Phys. Soc. **10**, 598 (1965).

[14] K. F. Cuff, M. R. Ellet, C. D. Kuglin, and L. R. Williams, in *Proceedings of the International Conference on Physics of Semiconductors* (Dunod Cie., Paris, 1964).

[15] D. L. Mitchell, E. D. Palik, and J. N. Zemel, in *Proceedings of the International Conference on Physics of Semiconductors* (Dunod, Cie., Paris, 1964).

[16] J. F. Butler and A. R. Calawa, in *Physics of Quantum Electronics Conference, Puerto Rico, 1965* (McGraw-Hill Book Co., New York, 1966), p. 458.

TABLE XIV. Elastic constants for PbS,[a] PbSe,[b] and PbTe,[b] in 10^{11} dyn/cm^2.

	c_{11}	c_{12}	c_{44}
PbS	11.4	3.4	2.5
PbSe	11.28	1.48	1.31
PbTe	10.69	0.89	1.31

[a] J. R. Burke, Jr., B. B. Houston, Jr., and R. S. Allgaier, Bull. Am. Phys. Soc. 6, 136 (1961).
[b] Reference 11.

The convergence of the matrix elements of momentum as a function of the number of APW vectors is of great significance. It was found that the value of some of these matrix elements did not converge satisfactorily with ten APW's. An attempt was made, in the case of PbS, to find a better value for momentum matrix elements by extrapolation. However, as it can be seen from Table XII, the extrapolated values tend to increase the effective masses.

The calculated values of g factors for PbTe and the wave functions of valence band were used by Bailey[17] to calculate the Knight shift for p-type PbTe. The theoretical value of 2.0×10^{-3} compares very well with the value of 2.34×10^{-3} measured by Weinberg and Callaway.[18]

C. Deformation Potentials

Ilisavskii[19] and Ilisavskii and Yakhkind[20] have measured the piezoresistance coefficient π_{ij} for n- and p-type PbTe, p-type PbSe, and n-type PbS. For a many-valley semiconductor, with the valleys on the [111] axis. Herring and Vogt[21] have derived the following relationship for the dimensionless elastoresistance coefficient m_{44}:

$$m_{44}=c_{44}\pi_{44}=\pm\tfrac{1}{9}(D_u/kT)[(\mu_l-\mu_t)/\mu], \qquad (5)$$

where μ_l and μ_t are the mobilities along the principal axes of the constant-energy ellipsoids, and $\mu=\frac{1}{3}(\mu_l-\mu_t)$, the average mobility. The plus and minus signs correspond to electrons and holes, respectively. Having measured the coefficient π_{44} and the elastic constant c_{44}, and knowing the anisotropy of the mobility $K=\mu_t/\mu_l$, one can obtain a value for D_u. Table XIV gives the experimentally measured value for the elastic constants of the lead salts.

TABLE XV. Comparison of theoretical values of D_u with experimental results from piezoresistance measurements.

	π_{44} (10^{-12} dyn^{-1}cm^2)	K	D_u (eV) Experiment	Theory
n-PbS	− 10.1	1.3	2.55	5.01
p-PbSe	57	2.0	5.5	4.76
n-PbTe	−107	4.33	3.6	8.29
p-PbTe	185	4.74	5.24	10.46

[17] P. T. Bailey, Sc.D. thesis, MIT, 1966 (unpublished).
[18] L. Weinberg and J. Callaway, Nuovo Cimento **24**, 190 (1962).
[19] Yu. V. Ilisavskii, Fiz. Tverd. Tela **4**, 918 (1962) [English transl.: Soviet Phys.—Solid State **8**, 1530 (1963)].
[20] Yu. V. Ilisavskii and E. Z. Yakhkind, Fiz. Tverd. Tela **4**, 1975 (1962) [English transl.: Soviet Phys.—Solid State **4**, 1447 (1963)].
[21] C. Herring and E. Vogt, Phys. Rev. **101**, 944 (1956).

TABLE XVI. Comparison of isotropic-deformation potential with the experimental results from the pressure variation of E_g.

	$\left(\frac{\partial E_g}{\partial P}\right)_T$ (10^{-6} eV/atm	D_{ISO} (eV) (conduction−valence) Experiment	Theory
PbS	−6.9	12.8	17.21
PbSe	−7.5	10.9	17.24
	−8.5	12.2	
PbTe	−9.0	11.5	11.5
	−8.0	10.2	

In the absence of experimental data regarding the anisotropy of mobility for PbS and PbSe, we shall assume that $\tau_l/\tau_t=1$ and thus $K=m_l/m_t$. Table XV shows the comparison of the experimental results at 300°K with the theory.

The fact that the theoretical values for D_u do not exactly agree with the experimental results may be due to the incorrectness of the assumption that the room-temperature mobility in lead salts is governed by acoustical-phonon scattering. In fact, a calculation by Efros[22] for PbS and PbTe shows that at $\kappa=0$, the optical branches of the phonon-dispersion spectrum come down to a frequency corresponding to 140 and 145°K, respectively. Thus at room temperature the optical modes are excited, and the mobility should be governed by scattering from optical phonons. Furthermore, the ionized-impurity scattering may have a part in the determination of mobility.

Averkin and Dombrouskaya[23] and Paul *et al.*[24] have experimentally measured the variation of the energy gap with hydrostatic pressure at constant temperature. Using the relationship

$$\mathbf{P}=c_{ij}\epsilon_{ij}=-(c_{11}+2c_{12})\epsilon, \qquad (6)$$

one can obtain D_{ISO} (Table XVI). The experimental values for $\partial E_g/\partial p$ predict that at 4.2°K, the energy gap would be reduced to zero at pressures of 40, 20, and 22 kbar for PbS, PbSe, and PbTe, respectively. However, this assumes a nonstrain-dependent deformation potential, an approximation which may not hold at these pressures.

ACKNOWLEDGMENTS

I am deeply grateful to Professor George W. Pratt, Jr., for his supervision and guidance of this work. Thanks are due to P. T. Bailey, N. de J. Parada, and J. E. Ripper Filho for many helpful discussions, and to D. L. Mitchell for pointing out a mistake in the calcalculation of the transverse effective mass. Acknowledgment is made of the use of the facilities of the MIT Computation Center.

[22] A. L. Efros, Fiz. Tverd. Tela **3**, 2065 (1961) [English transl.: Soviet Phys.—Solid State **3**, 1502 (1962)].
[23] A. A. Averkin and I. G. Dombrouskaya, Fiz. Tverd. Tela **4**, 366 (1962) [English transl.: Soviet Phys.—Solid State **5**, 66 (1963)].
[24] W. Paul, M. Demeis, and L. X. Finegold, in *Proceedings of the International Conference on Physics of Semiconductors, Exeter* (The Institute of Physics and the Physical Society, London, 1962), p. 212.